

Article

Microstructural Evolution and Tensile Properties of Al-Si Piston Alloys during Long-Term Thermal Exposure

Feng Xia ^{1,*}, Xiongbo Dong ², Jianli Wang ¹, Hongbo Duan ¹, Zhijun Ma ¹ and Minxian Liang ¹

¹ School of Materials and Chemical Engineering, Xi'an Technological University, Xi'an 710021, China; jlwang@xatu.edu.cn (J.W.); jason9890713@126.com (H.D.); sandy160922@126.com (Z.M.); minxianliang@126.com (M.L.)

² Shaanxi Railway Institute, Weinan 714000, China; xbdong_012@163.com

* Correspondence: xiafeng0811@163.com

Abstract: The present study investigated microstructural evolution and changes in tensile properties of an Al-Si piston alloy subjected to thermal exposures at 250 and 350 °C for 150, 300, and 500 h. Microstructural and nanoscale precipitates were characterized using a combination of high-angle annular dark field-scanning transmission electron microscopy (HAADF-STEM) images and scanning electron microscopy (SEM). The tensile testing was performed. The results demonstrated that the thermal exposure induced granulation of the δ -Al₃CuNi particles, alongside precipitation of the θ -Al₂Cu phase particles and AlCu clusters within the matrix. Specifically, an increase in the size and number density of the θ -Al₂Cu phase particles was observed with exposure time at 250 °C. Conversely, at 350 °C, the θ -Al₂Cu particles exhibited a gradual increase in size with prolonged thermal exposure, coupled with a decrease in their number density. AlCu clusters precipitated solely at a thermal exposure temperature of 350 °C, with precipitation intensifying over time. Moreover, a decrease in the alloy's tensile strength and an increase in elongation were noted after thermal exposure. Finally, the present study discussed the precipitation mechanisms of θ -Al₂Cu particles and AlCu clusters within the grains, suggesting that the AlCu clusters exerted a more effective strengthening effect compared to the θ -Al₂Cu particles.

Keywords: thermal exposure; Al-Si piston alloys; precipitates evolution; mechanical properties



Citation: Xia, F.; Dong, X.; Wang, J.;

Duan, H.; Ma, Z.; Liang, M.

Microstructural Evolution and Tensile Properties of Al-Si Piston Alloys

during Long-Term Thermal Exposure.

Metals **2024**, *14*, 535. <https://doi.org/10.3390/met14050535>

Academic Editor: Frank Czerwinski

Received: 29 March 2024

Revised: 27 April 2024

Accepted: 28 April 2024

Published: 30 April 2024



Copyright: © 2024 by the authors. Licensee MDPI, Basel, Switzerland. This article is an open access article distributed under the terms and conditions of the Creative Commons Attribution (CC BY) license (<https://creativecommons.org/licenses/by/4.0/>).

1. Introduction

The development of lightweight and high-performance pistons stands as a crucial strategy in advancing high-power, fuel-efficient diesel engines [1–3]. Near-eutectic multi-component Al-Si piston alloys containing elements such as Si, Cu, Ni, Mg, and Mn form many different intermetallic phases, which endows them with high specific strength, a low thermal expansion coefficient, and outstanding wear resistance. Thus, near-eutectic multicomponent Al-Si piston alloys are very attractive materials for the automotive industry [4–8]. However, throughout their service life, pistons frequently endure prolonged exposure to elevated temperatures ranging from 200 to 400 °C [9–11]. These sustained temperatures inevitably induce microstructural changes, thereby influencing the mechanical properties of the utilized alloys. Understanding the microstructural evolution and mechanical properties of Al-Si piston alloys at elevated temperatures is essential for ensuring the reliability of engine operations.

Near-eutectic multicomponent Al-Si piston alloys typically comprise Si (11–13 wt.%), Cu (3–5 wt.%), Mg (0.6–1.3 wt.%), Ni (0.5–3.0 wt.%), Fe (<1.3 wt.%), and various other microalloying elements, such as Co, Zr, Ti, Sc, and V, among others [12–14]. During the solidification of the alloy, metal elements like Cu, Mg, Ni, and Fe often form intermetallic compounds including ϵ -Al₃Ni, M-Mg₂Si, δ -Al₃CuNi, γ -Al₇Cu₄Ni, and Q-Al₅Cu₂Mg₈Si₆ [15–17]. These intermetallic compounds, owing to their distinctive structure and high thermal stability, significantly enhance the mechanical properties of

alloys. Particularly noteworthy is the interconnected three-dimensional network structure formed by eutectic Si and intermetallic compounds, which effectively reinforces the alloy matrix during deformation, thus imparting enhanced load-bearing capacity [18]. Furthermore, the Al matrix of the piston Al-Si alloys typically harbors numerous nano-scale precipitates, such as θ'' and θ' phase particles. These meta-stable particles with a nominal stoichiometry of Al₂Cu are considered to be the most effective in strengthening these alloys, and many studies have been made to tune the precipitation in Al-based alloys to optimize their mechanical properties [19–22].

The presence of second-phase particles can effectively hinder dislocation movement and grain boundary sliding at elevated temperatures, thereby bolstering the mechanical properties of Al-Si piston alloys at these temperatures [23,24]. However, as the temperature surpasses 250 °C, precipitates within the matrix, such as θ'' and θ' phase particles, rapidly coarsen and transform into larger, stable phases that are incoherent with the matrix, resulting in a marked decline in the strengthening effect [25–28]. For instance, Y. Sui et al. [29] have found that the second phase particles in an Al-12Si alloy remain unchanged after thermal exposure at 300 °C for 500 h. Conversely, T. Zeng et al. [30] have reported the complete disappearance of the θ' phase particles in the matrix after thermal exposure at 300 °C for 100 h in an Al-12Si-4Cu-1Mg-2Ni-0.2Gd alloy. Tian et al. [31] have studied the effects of thermal exposure on the microstructural and mechanical properties of Al-13Si-4Cu-2Ni-1Mg-0.25Mn piston alloy. They have found no alteration in the metallographic structure after thermal exposure at 350 and 420 °C for 1000 h. Additionally, they have identified new nanophase particles (Al₁₁Cu₅Mn₃) formed during the thermal exposure of the piston alloy. These particles significantly enhance the fatigue life of the investigated alloy. Despite some literature focusing on the intermetallics under thermal exposure, there remains a notable gap in systematic and comprehensive research on the microstructure damage evolution and mechanical properties degradation of piston alloys at the real elevated temperature, particularly regarding the formation and transformation mechanism of the phase particles under thermal exposure.

In this study, a peak-aged (T6 state) Al-Si piston alloy was subjected to different temperatures (250 °C and 350 °C) for various durations (150, 300, and 500 h). The microstructure during the thermal exposure process is characterized in detail by using SEM and TEM techniques. The evolution mechanism of the microstructure and mechanical properties of the alloy during thermal exposure was systematically discussed and analyzed.

2. Materials and Methods

2.1. Sample Preparation

The Al-Si piston alloy utilized in the present study was cut from the upper portion of the sand-casting piston assembly. Its average chemical composition was determined using an inductively coupled plasma optical emission spectrometry (ICP-OES) (Table 1). The alloy was initially solution treated at 500 °C for 8 h (quenching was performed in water), then aged at 215 °C for 6h in ambient air, and subsequently air-cooled to achieve the T6 state. Afterward, these samples were heated at different temperatures (250 and 350 °C) for different times (150, 300, and 500 h). The samples, equipment, and schematic diagram of the heat treatment procedure are illustrated in Figure 1.

Table 1. Average chemical composition of the piston alloy (wt. %).

Si	Cu	Mg	Ni	Fe	Zr	Ti	Sc	Ce	Al
11.5	3.9	0.9	2.25	0.16	0.18	0.17	0.18	0.25	Bal.

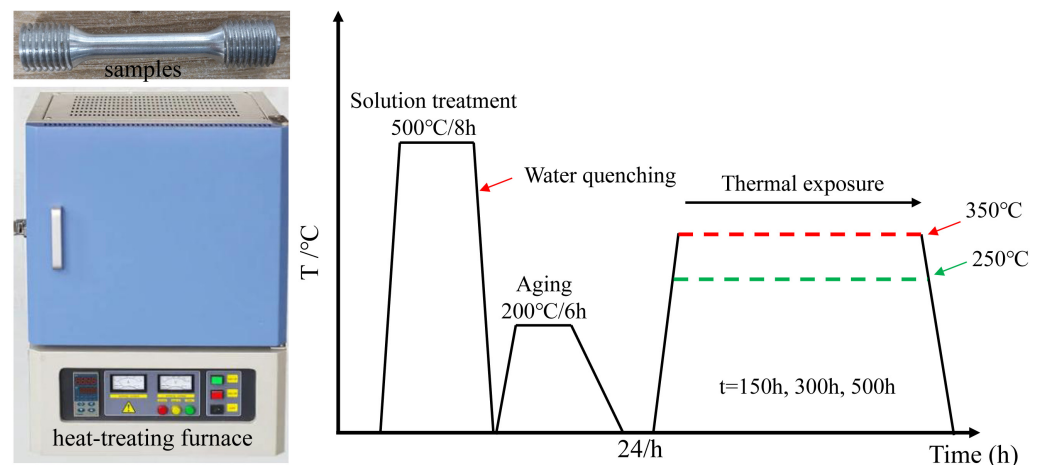


Figure 1. The samples, equipment, and schematic diagram of the heat treatment process.

2.2. Microstructural Examination

For microstructural observation, the alloy specimens were ground and polished using standard metallographic techniques. The samples were etched with a solution composed of nitric acid, hydrochloric acid, hydrofluoric acid, and water (in a volume ratio of 2.5:1.5:1.0:95.0). The microstructures were observed using a Zeiss Gemini 500 FEG SEM equipped with energy dispersive system (Zeiss, Jena, Germany), and transmission electron microscopy (TEM). The composition of the intermetallic compounds within the samples was estimated via EDS analysis. The evolution of the microstructure under varying thermal exposure conditions was investigated using a transmission electron microscopy (TEM Talos F200x, Thermo Fisher Scientific, Waltham, MA, USA) operating at 200 kV. TEM samples were prepared by following the standard ion thinning procedure. ImageJ 1.8.3 software was employed to quantitatively determine the sizes of the observed phase particles in both SEM and TEM micrographs. A total of 10 micrographs were analyzed for each sample group, and the average value was considered as the experimental result.

2.3. Tensile Testing

For the tensile test, the standardized tensile samples (see Figure 2) were prepared from the piston by electrical discharge machining, and the room-temperature tensile testing was conducted using a servo-hydraulic Instron testing machine (Instron 4206, Instron Corporation, Norwood, MA, USA) with a crosshead speed of 1.5 mm/min. Additionally, tensile testing was carried out at 350 °C, employing a crosshead speed of 1 mm/min. For each testing condition, tensile properties (tensile strength and elongation at break) were determined after analyzing three dog-bone-shaped specimens with dimensions of the gauge section of $\text{Ø}6 \text{ mm} \times 60 \text{ mm}$.

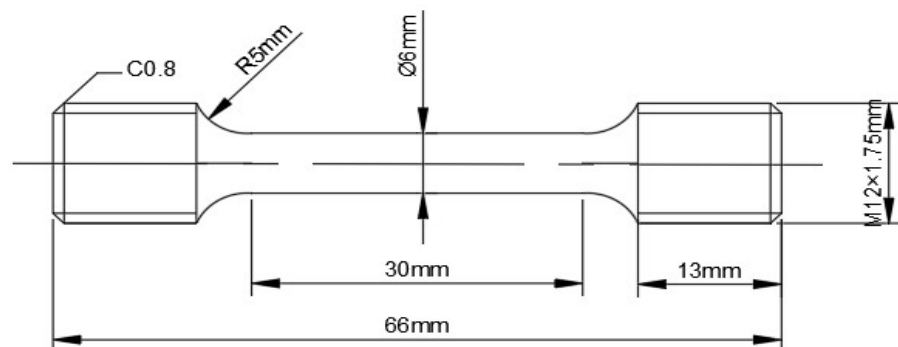


Figure 2. Dimension of tensile test samples.

3. Results

3.1. Microstructural Evolution

Figure 3 displays representative SEM and TEM micrographs of the Al-Si piston alloy samples in the T6 state. EDS point analyses were performed on the phase particles, as shown in Figure 3a,b. In these figures, the measurement locations are designated with numbers between 1 and 6, whereas the measurement results are presented in Table 2. Drawing upon prior research concerning the morphology and composition of intermetallic compounds in Al-Si piston alloys [24,26], the chemical formulas of each phase particle were derived. The three-dimensional network structure, comprising primary Si, eutectic Si, δ -Al₃CuNi, and Q-Al₅Cu₂Mg₈Si₆ phase particles, observed in Figure 3a, served to stabilize grain boundaries during deformation, thereby enhancing the mechanical properties of the alloy. In Figure 3b, a high magnification image of the matrix microstructure in the T6 state revealed solely an Al matrix (indicated by red arrows), without the presence of tiny precipitates. Figure 3c demonstrates that the aging precipitates in the T6-treated Al-Si piston alloy samples predominantly consisted of flaky strengthening θ'' and θ' phase particles, as confirmed by the diffraction pattern in the inset of Figure 3c. These two strengthening phase particles exhibited coherent or semi-coherent interfaces with the matrix, requiring higher stress levels to disrupt the interface between the particles and the matrix, thus reducing the likelihood of crack formation during the deformation of the alloy [32].

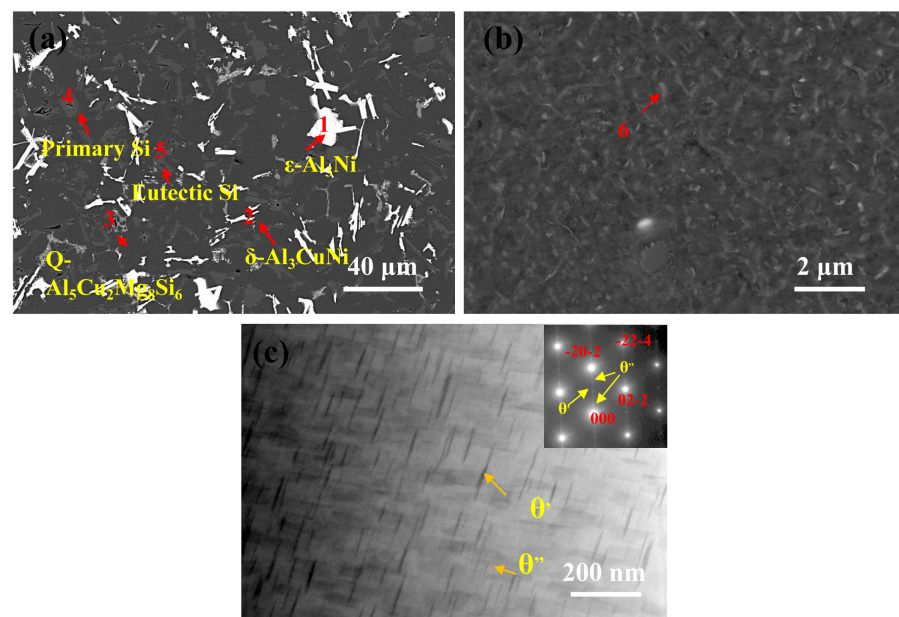


Figure 3. The microstructure of the alloy in the T6 state: (a) SEM micrograph, (b) High magnification SEM micrograph of the matrix, (c) TEM micrographs.

Table 2. EDS point analyses performed on sites shown in Figure 3a,b.

EDS Spectrum Number	Fraction of Elements Detected in Each EDS Spectrum (at.%)									Estimated Phase Particles
	Al	Si	Cu	Mg	Ni	Fe	Sc	Zr	Ti	
1	71.7	1.3	~	~	25.9	0.6	0.3	~	0.2	ϵ -Al ₃ Ni
2	58.8	0.4	18.9	0.1	21.4	0.2	0.1	0.1	~	δ -Al ₃ CuNi
3	25.1	30.5	7.4	36.8	0.1	~	~	0.1	~	Q-Al ₅ Cu ₂ Mg ₈ Si ₆
4	3.6	95.6	0.4	~	0.2	~	~	0.2	~	Primary Si
5	9.6	88.7	1.2	0.3	0.1	0.1	~	~	~	Eutectic Si
6	96.5	0.3	2.8	0.2	~	0.1	~	~	0.2	Al matrix

Figure 4a–f illustrate SEM micrographs of the alloy samples after thermal exposure at 250 and 350 °C for 150, 300, and 500 h, respectively. It is apparent that the granulation of the δ -Al₃CuNi phase intensified with longer thermal exposure. Moreover, as the thermal exposure temperature rose from 250 to 350 °C, the granulation of the δ -Al₃CuNi phase became more prominent. This granulation disrupted the three-dimensional network structure, adversely affecting the alloy's properties. In addition, high-magnification SEM micrographs in Figure 4 revealed the formation of numerous fine precipitates within the matrix after thermal exposure between 250 and 350 °C. Such fine precipitates were absent in the matrix structure of the T6 alloy samples (Figure 3b). EDS results (Figure 4g) indicated that the precipitates within the matrix primarily consisted of Al and Cu elements. Based on the elemental atomic fractions of Al and Cu, these precipitates could be preliminarily identified as the θ -Al₂Cu phase. It is evident that the size and density of θ -Al₂Cu phase particles increased with prolonged exposure time at an exposure temperature of 250 °C. At the exposure temperature of 350 °C, the size of the θ -Al₂Cu phase particles became much larger than that at 250 °C, while the density decreased with increasing exposure time. Figure 4 demonstrates that during the thermal exposure process at both 250 and 350 °C, the phase transition primarily occurred in the δ -Al₃CuNi phase and the matrix.

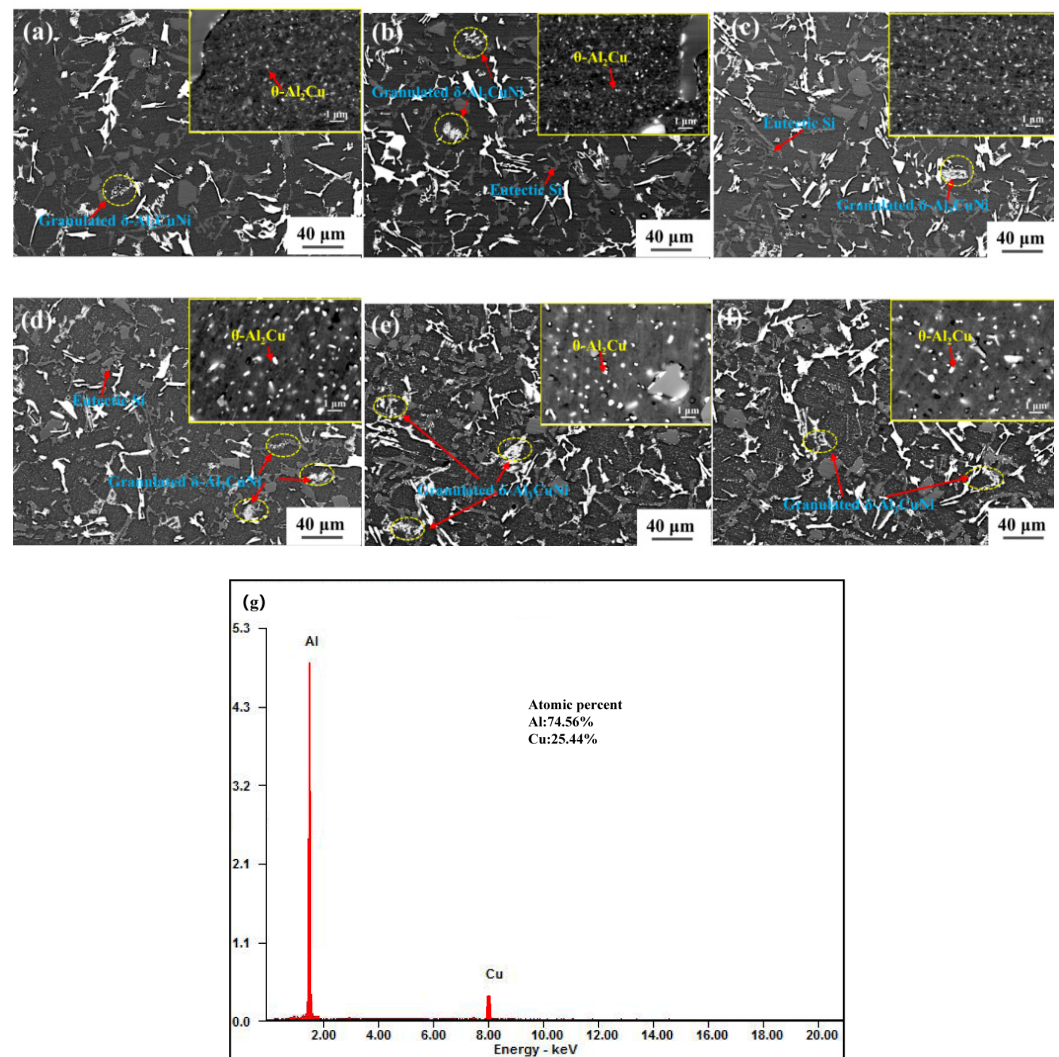


Figure 4. Microstructure of the Al-Si piston alloy samples after thermal exposure at (a–c) 250 and (d–f) 350 °C for (a,d) 150, (b,e) 300, and (c,f) 500 h. The insets are high-magnification SEM micrographs of the matrix, while (g) is the typical EDS spectrum taken from the θ -Al₂Cu particles shown in the insets.

To clearly illustrate the precipitation evolution behavior of the θ -Al₂Cu phase particles, the size and number density (Nv) of these particles were quantitatively measured, and the results are presented in Figure 5. It is obvious that the size of the θ -Al₂Cu phase particles gradually increased with increasing exposure temperature and time. Furthermore, the size of the θ -Al₂Cu particles at 350 °C was significantly larger than that at 250 °C. This was mainly due to the faster diffusion rate of Cu atoms at elevated temperatures, resulting in intensified coarsening of the θ -Al₂Cu phase particles. Moreover, at 250 °C, the number density of the θ -Al₂Cu phase particles increased with the exposure time, while it exhibited the opposite trend at 350 °C. This may be attributed to the dissolution of the small-sized θ -Al₂Cu phase particles at higher exposure temperatures.

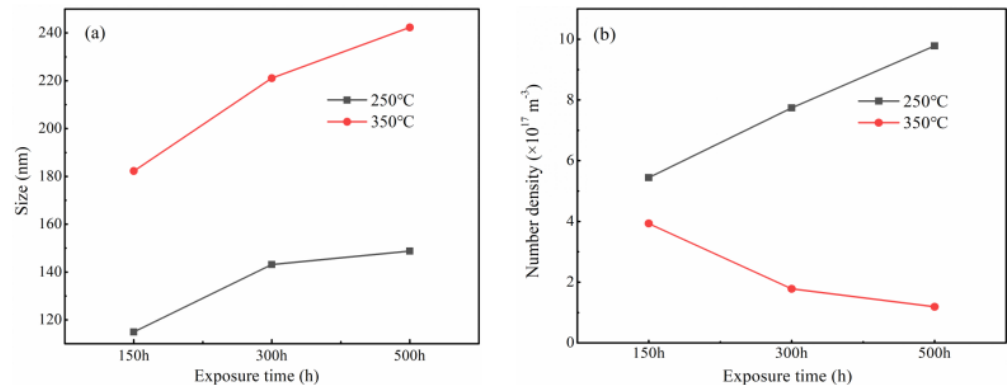


Figure 5. Evolution of (a) size and (b) number density of θ -Al₂Cu phase particles under different conditions of thermal exposure.

Figure 6 shows representative TEM micrographs of the Al-Si piston alloy samples subjected to thermal exposure at 250 and 350 °C for different time intervals. Figure 6a–e reveal the presence of flaky θ' phase particles within the matrix during thermal exposure at 250 °C. According to the selected area electron diffraction (SAED) analysis (the inset of Figure 6a), these flake-like precipitates were assigned to θ' phase. Additionally, the presence of some bulky phase precipitates was observed. According to SAED analysis (the inset of Figure 6b), these precipitates were ascribed to the θ phase. These bulky θ phase particles corresponded to the fine precipitates observed in the matrices shown in the insets of Figure 4. Figure 6a–c demonstrate that during thermal exposure at 250 °C, θ' phase remained present in the matrix as exposure time increased. Moreover, the size and number density of the θ phase particles increased with prolonged exposure time, which is consistent with observations in Figure 5.

Figure 6d–f show typical TEM micrographs of the alloy samples subjected to thermal exposure at 350 °C for various durations. It is evident that the θ' phase particles disappeared, forming a bulky θ phase compared to the alloy samples thermally exposed at 250 °C. In addition, the density of θ phase particles in the alloy gradually diminished with increasing thermal exposure time, aligning with the quantitative analyses from SEM micrographs shown in Figure 5. Furthermore, in addition to the θ phase particles in the matrix, some bulk phase particles measuring approximately 50 nm in size and point-like particles measuring around 7 nm in size were also observed, as indicated by red dashed boxes in Figure 6.

Compositional analyses of the bulk and point-like particles were conducted using EDS energy spectra of TEM, and the results are shown in Figure 7. It is evident that both phase particles were composed of Al and Cu elements, with the bulk phase particles exhibiting significantly higher Cu content compared to the point-like phase particles. Importantly, the Cu content surpassed the maximum solubility of Cu in Al (~5.65%), indicating the formation of a new AlCu phase.

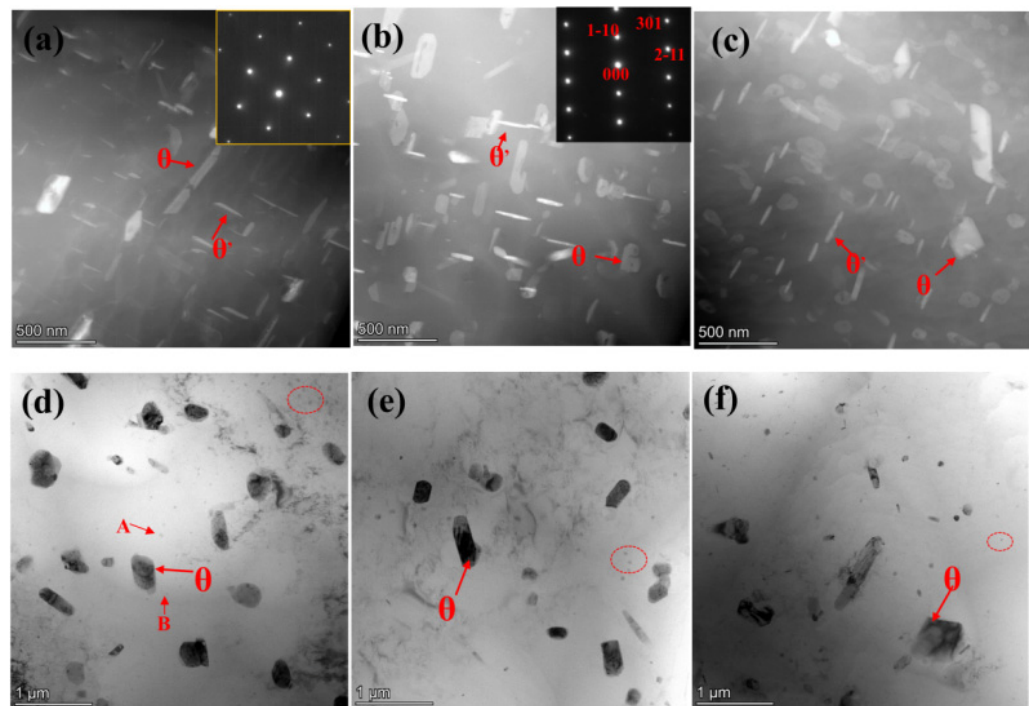


Figure 6. TEM micrographs of the alloy samples after thermal exposure at (a–c) 250 and (d–f) 350 °C for (a,d) 150, (b,e) 300, and (c,f) 500 h. The insets are SAED patterns.

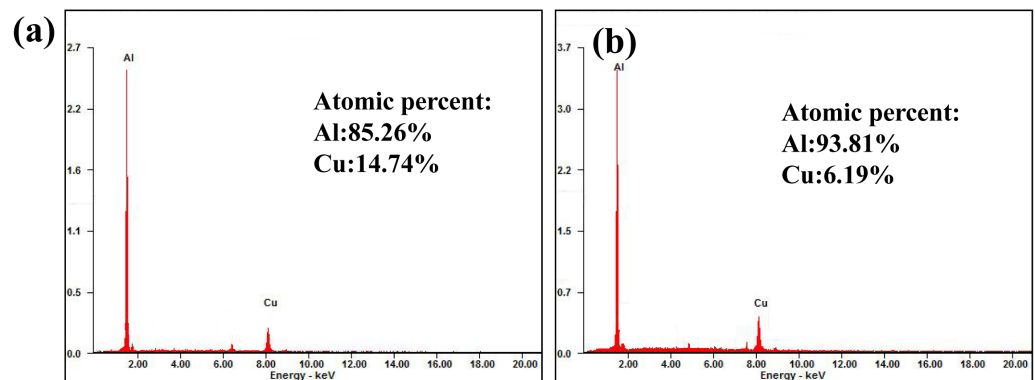


Figure 7. EDS spectra of the precipitated phase particles at (a) A and (b) B sites designated in Figure 6d.

The bulk and point-like AlCu phases precipitated after thermal exposure at 350 °C were observed using the HAADF-STEM mode, and the results are shown in Figure 8. The unique Z-contrast imaging capability of the HAADF-STEM mode effectively eliminates the adverse effects of dislocations and other defects on the observation, enabling a clear reflection of the real morphology and distribution of the AlCu phase. It is obvious that with the extension of thermal exposure time, the presence of the bulk AlCu phase particles gradually decreased, while the presence of point-like AlCu phase particles increased. The distinct contrast observed in Figure 8, with the central region of the bulk AlCu phase particles appearing brighter and the edges darker, suggested a concentration gradient of Cu atoms within the bulk AlCu phase particles. Specifically, the brighter center indicated a higher Cu atomic concentration compared to the darker edges. This contrast variation likely arose due to the diffusion of Cu atoms within the bulk AlCu phase during thermal exposure. As exposure time increased, Cu atoms diffused into the surrounding matrix, leading to a gradual disappearance of the bulk AlCu phase and the formation of a smaller point-like AlCu phase. Furthermore, the relatively lower Cu content in the AlCu phase

resulted in its reduced contrast in the HAADF-STEM morphology images (TEM Talos F200x, Thermo Fisher Scientific, Waltham, MA, USA). This diminished contrast made it challenging to quantitatively analyze the morphology and distribution of the AlCu phase.

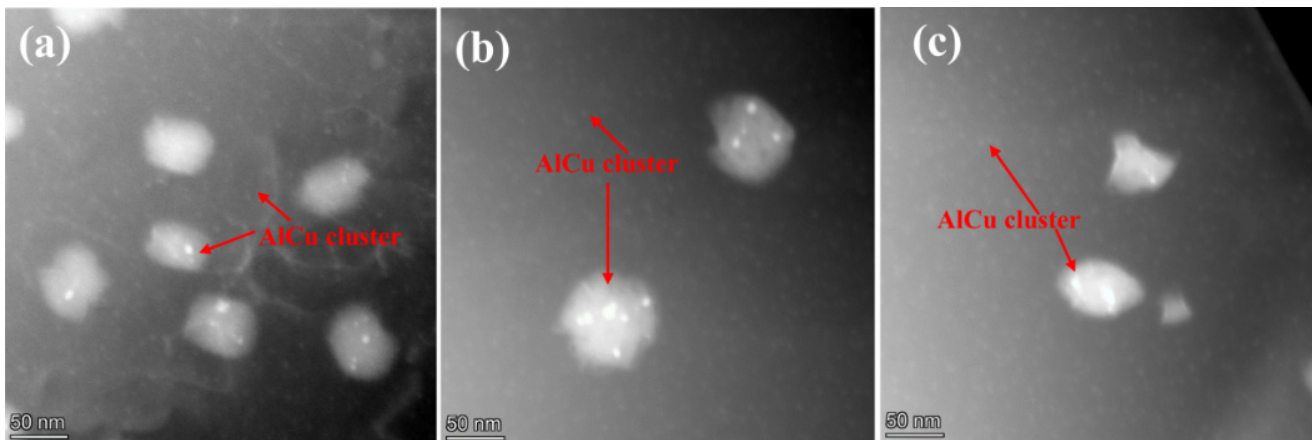


Figure 8. Representative high-magnification HAADF-STEM micrographs of the alloy samples after thermal exposure at 350 °C for (a) 150, (b) 300, and (c) 500 h.

Figure 9a,b depict the HAADF-STEM morphology, elemental surface distribution, and line scanning results of the Al-Si piston alloy samples after thermal exposure at 350 °C for 150 h and 500 h, respectively. The line scanning results were conducted along the direction of the red dotted line in the HAADF-STEM morphology image. Given that the newly precipitated AlCu phase consisted solely of Al and Cu elements, only changes in Al and Cu elements were considered. In Figure 9a, the STEM-EDS elemental maps of Cu clearly revealed the presence of bulk AlCu precipitates, while the point-like AlCu phase exhibited an insufficient signal-to-noise ratio to delineate its enrichment due to its lower Cu content. Figure 9b demonstrates significant fluctuations in Cu composition across the bulk AlCu phase, whereas fluctuations were less pronounced in other regions of the matrix, primarily due to the higher Cu content of the bulk AlCu phase. Figure 9c displays the AlCu phase and its elemental plane distribution in the matrix after 500 h of thermal exposure. Although some Cu enrichment was visible, the signal-to-noise ratio was insufficient to delineate the AlCu precipitate. Figure 9d highlights obvious composition fluctuation in the Cu element, indicating the formation of Cu element segregation within the matrix. Notably, the fluctuation frequency of the Cu element in Figure 9b was much lower than that in Figure 9d. This fact suggested that more AlCu phases were formed during thermal exposure at 350 °C for 500 h compared to 150 h, which is consistent with the HAADF-STEM observation in Figure 8.

In Figure 10a, the TEM image displays the alloy sample after thermal exposure at 250 °C for 300 h, revealing numerous short rod-shaped θ' phase particles and massive θ phase particles in the matrix. High-resolution TEM (HRTEM) analysis of the θ and θ' phase particles in Figure 10a along the $[011]_{\text{Al}}$ band axis is presented in Figure 10b and c, respectively. In Figure 10b, the HRTEM analysis of the θ phase particle indicated that it lacked a specific crystal plane relationship with the Al matrix, exhibiting an incoherent interface. In Figure 10c, it is evident that the atomic arrangement of the long face of θ' phase particle was consistent with that of the Al matrix, indicating a coherent interface. However, the atomic arrangement of its broad face significantly differed from that of the Al matrix, with periodic bright stripes apparent. The yellow dashed boxes 1 and 2 in Figure 10c represent the matrix and the broad face of the θ' phase particle, respectively. Their corresponding fast Fourier transform (FFT) and magnified images are shown in Figure 10d and e and Figure 10f and g, respectively. The results showed that the matrix exhibited a two-dimensional lattice without distortion, indicative of an FCC structure. On the other hand, the broad surface of the θ' phase exhibited a long-period structure

composed of the orderly arrangement of stacking faults (Figure 10e,g). The generation of stacking faults was attributed to the large thermal stress generated during thermal exposure. Moreover, the generation of stacking faults is generally accompanied by dislocations, which can act as diffusion channels for Cu atoms [33]. Consequently, the stacking faults generated by the broad face of the θ' phase facilitated the precipitation of Cu atoms on the surface of the θ' phase and accelerated the coarsening efficiency.

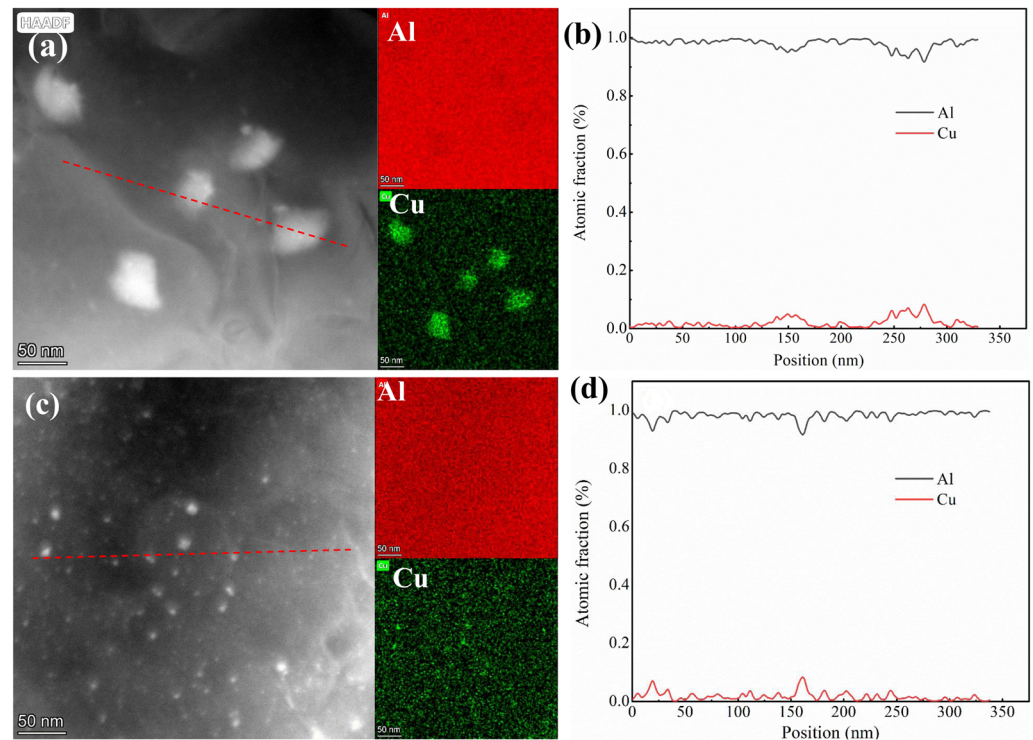


Figure 9. (a) HAADF-STEM micrograph of the alloy samples thermally exposed to temperature of 350 °C for 150 h with its Al and Cu elemental maps, (b) distribution of Al and Cu along the red dotted line in (a), (c) HAADF-STEM micrograph of the alloy samples exposed to temperature of 350 °C for 500 h with its Al and Cu elemental maps, and (d) distribution of Al and Cu along the red dotted line in (c).

In Figure 11a, the TEM micrograph displays the alloy sample subjected to thermal exposure at 350 °C for 150 h, with the red dashed boxes 1 and 2 highlighting the point-like and bulk AlCu phases, respectively. SAED was performed on the red dotted boxes 1 and 2 in Figure 11a, and the results are presented in Figure 11b and 11d, respectively. The two sets of diffraction spots showed no additional diffraction spots apart from those of Al, indicating an insignificant lattice structure between the AlCu phases and the Al matrix. High-resolution observations of the red dotted boxes 1 and 2 in Figure 11a along the $[011]_{\text{Al}}$ band axis are shown in Figure 11c and 11e, respectively. The HRTEM images in Figure 11c,e clearly revealed that the sizes of the two AlCu phase particles were 2–5 and 50 nm, respectively. Magnified HRTEM images of the yellow wireframe area in Figure 11c,e are shown in Figure 11f and 11g, respectively. The insets in Figure 11f,g display their corresponding FFT images, wherein only Al spots were observed. Additionally, both types of AlCu particles exhibited coherence with the Al matrix, as shown in Figure 11f,g. Therefore, it is reasonable to speculate that Cu atoms randomly replaced the lattice positions of Al atoms in the matrix, resulting in the formation of the AlCu phase. In summary, these AlCu phases were recognized as AlCu clusters.

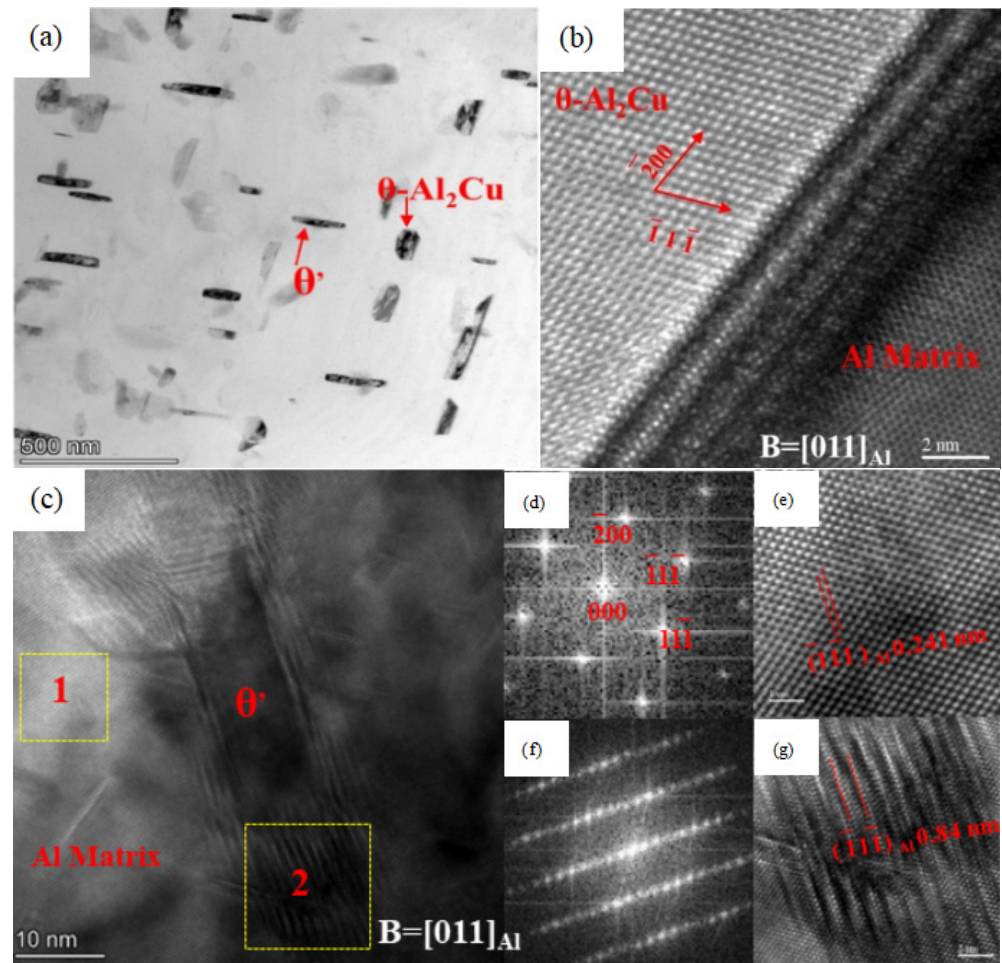


Figure 10. HRTEM micrographs of the Al-Si piston alloy samples thermally exposed at 250 °C for 300 h. (a) TEM morphology of the precipitated phase particles within the matrix, (b) high-resolution image of the [011]Al oriented θ -Al₂Cu phase particle within the matrix, (c) high-resolution image of the [011]Al oriented θ' -Al₂Cu phase particle within the matrix, (d,e) inverse Fourier transform images of the yellow-dashed wireframes depicted as 1 and 2 regions in figure (c), and (f,g) magnified images of the yellow-dashed wireframe depicted as 1 and 2 regions in figure (c).

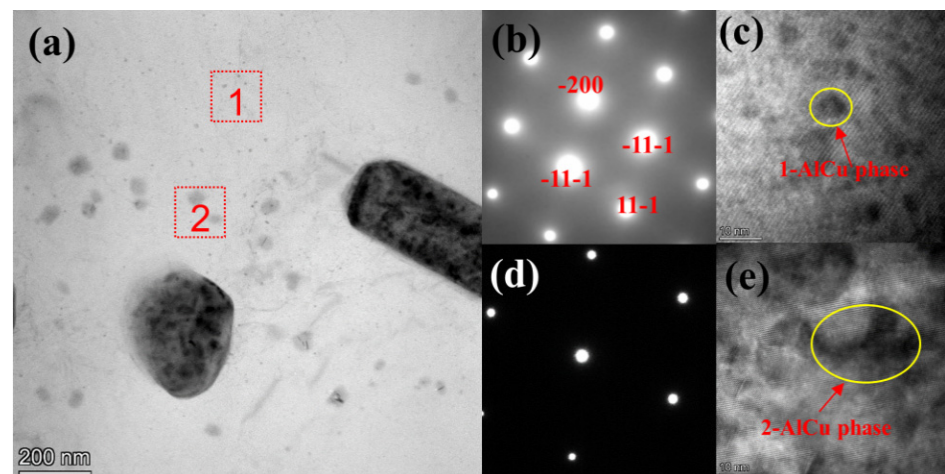


Figure 11. Cont.

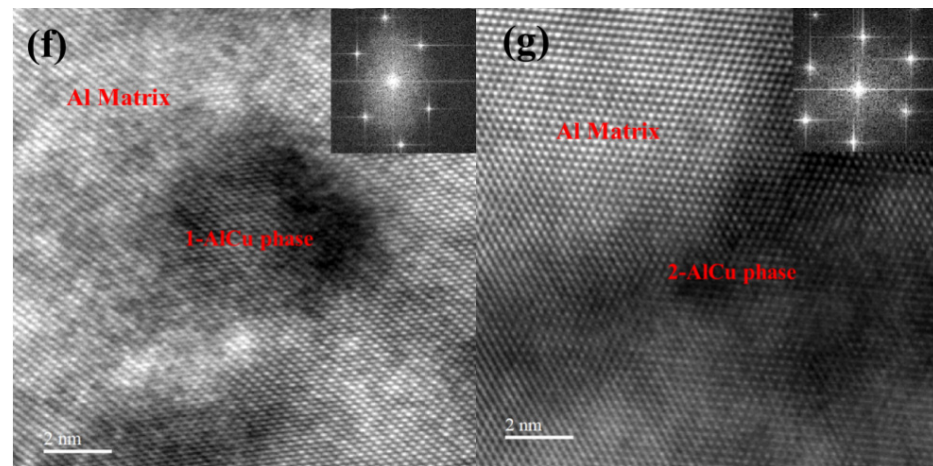


Figure 11. HRTEM images of the alloy sample thermally exposed at 350 °C for 150 h: (a) TEM morphology of the matrix precipitates, (b) SAED of the area 1 in the red dashed box in (a), (c) high-resolution image of the red dashed box area 1 in (a), (d) SAED of the red dashed box 2 area in (a), (e) high-resolution image of the red dashed box 2 area in (a), (f) magnified image of the area marked with the red arrow in (c) and the inset is its FFT image, (g) magnified image of the area marked with the red arrow in (e) and the inset is its FFT image.

3.2. Tensile Properties

Figure 12 depicts the changes in the tensile properties of the Al-Si piston alloy specimens in the T6 state after thermal exposure at 250 and 350 °C for 150, 300, and 500 h, respectively. Additionally, for comparison, the tensile strength and elongation of the T6 tempered Al-Si piston alloy at 25 and 350 °C were also provided. The tensile strength and elongation at 25 °C were determined to be 300 MPa and 1%, respectively, whereas at 350 °C, they were measured to be 98 MPa and 7.0%. In Figure 12a, the tensile strength of the alloy specimens significantly decreased after thermal exposure relative to the T6 state, with the most significant reduction observed at a thermal exposure temperature of 350 °C. This decrease in strength was primarily attributed to the transformation of θ' to θ and the disruption of the rigid three-dimensional network structure caused by the granulation of the δ -Al₃CuNi phase. At a thermal exposure temperature of 250 °C, the tensile strength decreased slightly for two reasons. The first was due to the weaker granulation of the δ -Al₃CuNi phase. The second was due to the presence of the coherent interface between θ' phase and the alloy matrix. As the exposure time at 250 °C increased, the tensile strength of the alloy specimens further decreased. Interestingly, at a higher thermal exposure temperature of 350 °C, there was a slight increase in tensile strength with extended exposure time, as shown in Figure 12a. This increase could be attributed to the strengthening effect of AlCu clusters.

Figure 12b illustrates the effects of exposure temperature (250 and 350 °C) and exposure time (150, 300, and 500 h) on the elongation at break obtained at 25 and 350 °C. It is apparent that elongation at break gradually increased with thermal exposure temperature and time. This behavior could be attributed to the reduction in the number density of precipitated phase particles. The decrease in the number density of the precipitates increased the interparticle spacing, making it easier for dislocations to bypass, thus reducing the likelihood of stress concentration during the deformation.

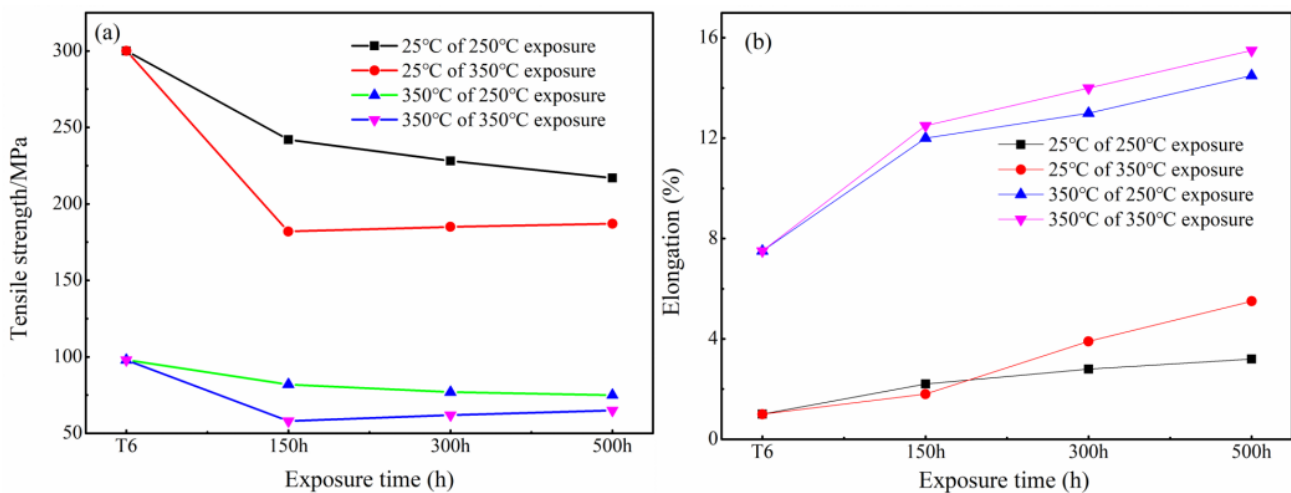


Figure 12. The results of tensile testing performed at 25 and 350 °C on the alloy specimens previously subjected to different thermal exposure conditions: (a) tensile strength and (b) elongation.

4. Discussion

In the present study, the thermal exposure of peak-aged (T6 state) Al-Si piston alloys at 250 and 350 °C led to certain changes in the alloy microstructure, such as granulation of the δ -Al₃CuNi phase particles, nucleation and growth of new θ -Al₂Cu phases, and the formation of AlCu clusters. From a thermodynamic perspective, these phase changes occurred due to alterations in the microstructure equilibrium state caused by prolonged thermal exposure [34]. Therefore, analyzing the phase transition mechanism required considering the effects of temperature and time on the material's internal state.

In Al-Si piston alloys, the δ -Al₃CuNi phase is an intermetallic compound with a high hardness and a high elastic modulus. Compared to the matrix, the elastic modulus of such intermetallic compounds is significantly higher at the same temperature [35]. Generally, for phases with high elastic modulus, even slight changes in atomic spacing or arrangement can lead to a sharp increase in their free energy, several times to dozens of times higher than that of the matrix [36]. The δ -Al₃CuNi phase, having the highest elastic modulus among the intermetallic compounds in the Al-Si piston alloy, exhibits the largest free energy difference compared to the matrix at the same temperature, resulting in the most significant phase transition driving force. Solid state transition occurs based on atomic migration. In this case, Cu atoms, with a high diffusion coefficient in the Al matrix, continuously diffused from the high-energy state δ -Al₃CuNi phase into the matrix at elevated temperatures, leading to granulation of the δ -Al₃CuNi phase particles.

The small particles produced by the granulation of the high-energy δ -Al₃CuNi phase particles had higher free energy and were more easily redissolved into the matrix, causing the matrix to become supersaturated. This supersaturation resulted in the atom segregation or the re-nucleation of precipitates in the alloy, even at higher temperatures. An Al matrix with a certain degree of solute saturation existed in a high-energy state. If the re-precipitated phases like the GP zone, θ'' , or θ' phase with a coherent or semi-coherent interface with the matrix occur, the free energy of the matrix increases further. However, the formation of the θ phase, which lacks a coherent relationship with the parent phase of the Al matrix and is formed at grain boundaries, phase boundaries, or defects, can help reduce the free energy of the Al matrix. Figure 4 demonstrates that most of the θ -Al₂Cu phase particles were distributed at the interface of the Si phase particles, δ -Al₃CuNi phase particles, and the matrix, confirming this point. During thermal exposure at 250 °C, the increase in the internal energy of the θ -Al₂Cu phase was insufficient for it to redissolve into the matrix, resulting in a gradual increase in the number density of the θ -Al₂Cu phase particles with thermal exposure time. However, when the thermal exposure temperature increased to 350 °C, the size of the θ -Al₂Cu phase particles increased while the number density

decreased with thermal exposure time due to the Ostwald ripening, where larger particles grew at the expense of smaller ones.

Apart from the formation of the θ -Al₂Cu phase, many AlCu clusters also precipitated in the alloy at a thermal exposure temperature of 350 °C. This formation of AlCu clusters may be attributed to the formation of free Cu atoms in the matrix, which aggregate from low-concentration regions to high-concentration regions. Generally, traditional solute clusters form from supersaturated solid solutions like GP zones. Therefore, the formation of AlCu clusters in the present study differed from the formation of traditional clusters and it was the first observation of such clusters during the thermal exposure of Al-Si piston alloys at elevated temperatures.

On one hand, the decrease in the strength of the alloy during thermal exposure could be attributed to two main processes: the transformation of the θ' to the θ phase particles and granulation of the δ -Al₃CuNi phase particles, leading to the destruction of the three-dimensional rigid structure. On the other hand, the precipitation of intragranular θ -Al₂Cu phase particles and AlCu clusters was beneficial to the alloy strength. The change in the strength of the alloy during thermal exposure was the combined result of these processes. In the present study, at a thermal exposure temperature of 250 °C, the tensile strength continued to decrease with increasing exposure time. During this period, numerous θ -Al₂Cu phase particles existed in the matrix. Only a moderate increase in the granulation of δ -Al₃CuNi and the coarsening of θ' occurred. This means that the θ -Al₂Cu phase particles produced a little enhancement effect on the tensile strength of the alloy specimens. However, at a thermal exposure temperature of 350 °C, the tensile strength slightly increased with increasing thermal exposure time. During this period, numerous AlCu clusters existed in the matrix, whereas the presence of the θ -Al₂Cu phase particles continued to decrease. This suggested that under these conditions, AlCu clusters significantly enhanced the tensile strength of the Al-Si piston alloy compared to the effect of the θ -Al₂Cu phase.

5. Conclusions

The investigation into the effects of thermal exposure on the microstructural evolution and tensile properties of the Al-Si piston alloy yielded several key findings:

(1) The δ -Al₃CuNi phase underwent granulation during the thermal exposure process, with the degree of granulation increasing gradually with both temperature and time of thermal exposure. This granulation was primarily attributed to the higher increase in free energy of the δ -Al₃CuNi phase particles compared to the matrix at elevated temperatures.

(2) At a thermal exposure temperature of 250 °C, both the size and number density of the θ -Al₂Cu phase increased with thermal exposure time. Conversely, at 350 °C, the size of the θ -Al₂Cu phase particles increased while the number density decreased over time, a phenomenon assigned to Cu atom diffusion from the matrix and Ostwald ripening.

(3) Precipitation of θ -Al₂Cu phase particles and AlCu clusters occurred during thermal exposure. θ -Al₂Cu phase particles preferentially precipitated from grain boundaries, with exposure temperature playing a significant role in their precipitation. AlCu clusters, on the other hand, only precipitated at a thermal exposure temperature of 350 °C due to the aggregation of Cu atoms from low- to high-concentration regions. The diffusion of Cu atoms during the coarsening of θ' to θ predominantly depended on stacking faults induced by thermal stress.

(4) The tensile strength of the alloy decreased while the elongation at break increased after thermal exposure. The strengthening effect of the θ -Al₂Cu and AlCu clusters can alleviate effectively the decrease in tensile strength of the Al-Si piston alloy. The AlCu clusters exhibited a much greater strengthening effect compared to the θ -Al₂Cu phase particles under investigated conditions.

Author Contributions: Conceptualization, F.X. and M.L.; investigation, X.D.; writing—original draft preparation, J.W.; writing—review and editing, H.D.; supervision, Z.M. All authors have read and agreed to the published version of the manuscript.

Funding: This research was funded by The Youth Innovation Team of Shaanxi Universities grant number [K20220185], Shaanxi key research and development program grant number (2020ZDLGY13-01). The APC was funded by the Shaanxi Key Research and Development Program.

Data Availability Statement: The data presented in this study are available on request from the corresponding author. The data are not publicly available due to privacy.

Acknowledgments: This work was supported by the Youth Innovation Team of Shaanxi Universities (K20220185), Shaanxi key research and development program (2020ZDLGY13-01).

Conflicts of Interest: The authors declare no conflict of interest.

References

1. Mirzaee-Moghadam, M.; Lashgari, H.R.; Zangeneh, S.; Rasaee, S.; Seyfor, M.; Asnavandi, M.; Mojtahedi, M. Dry sliding wear characteristics, corrosion behavior, and hot deformation properties of eutectic Al–Si piston alloy containing Ni-rich intermetallic compounds. *Mater. Chem. Phys.* **2022**, *279*, 125758.
2. Liu, Y.X.; Xiong, S.M. Research Progress on Thermal Conductivity of High-Pressure Die-Cast Aluminum Alloys. *Metals* **2024**, *14*, 370. [\[CrossRef\]](#)
3. Cao, H.S.; Liu, F.J.; Li, H.; Qi, F.G.; Ouyang, X.P.; Zhao, N.; Liao, B. High temperature tribological performance and thermal conductivity of thick Ti/Ti-DLC multilayer coatings with the application potential for Al alloy pistons. *Diam. Relat. Mater.* **2021**, *117*, 108466. [\[CrossRef\]](#)
4. Liu, L.; Tang, C.W.; Feng, W.; Yu, H.L.; He, Z.B.; Chu, X.C.; Wang, P.; Yang, Z.; Guo, Y.C. Effect of Cu addition on the microstructure, thermal physical properties and cyclic ablation of C/C-AlSi composite. *J. Alloys Compd.* **2023**, *969*, 172378. [\[CrossRef\]](#)
5. Han, L.; Sui, Y.; Wang, Q.; Wang, K.; Jiang, Y. Effects of Nd on microstructure and mechanical properties of cast Al–Si–Cu–Ni–Mg piston alloys. *J. Alloys Compd.* **2017**, *695*, 1566–1572. [\[CrossRef\]](#)
6. Efsan, M.N.; Kong, H.J.; Kok, C.K. Review: Effect of alloying element on Al–Si alloys. *Adv. Mater. Res.* **2013**, *845*, 355–359. [\[CrossRef\]](#)
7. Mfusi, B.J.; Popoola, P.A.; Mathe, N.R. Optimisation of the Heat Treatment Profile for Powder-Bed Fusion Built AlSi10Mg by Age Hardening and Ice-Water Quenching. *Metals* **2024**, *14*, 292. [\[CrossRef\]](#)
8. Jung, J.G.; Lee, S.H.; Lee, J.M.; Cho, Y.H.; Kim, S.H.; Yoon, W.H. Improved mechanical properties of near-eutectic AlSi piston alloy through ultrasonic melt treatment. *Mater. Sci. Eng. A* **2016**, *669*, 187–195. [\[CrossRef\]](#)
9. Javidani, M.; Larouche, D. Application of cast Al–Si alloys in internal combustion engine components. *Int. Mater. Rev.* **2014**, *59*, 132–158. [\[CrossRef\]](#)
10. Ye, H. An overview of the development of Al–Si–Alloy based material for engine applications. *J. Mater. Eng. Perform.* **2003**, *12*, 288–297. [\[CrossRef\]](#)
11. Samuel, E.; Tahiri, H.; Samuel, A.M.; Samuel, F.H. Heterogenous Grain Nucleation in Al–Si Alloys: Types of Nucleant Inoculation. *Metals* **2024**, *14*, 271. [\[CrossRef\]](#)
12. Kasprzak, W.; Chen, D.L.; Shaha, S.K. Heat treatment development for a rapidly solidified heat resistant cast Al–Si alloy. *J. Mater. Eng. Perform.* **2013**, *22*, 1838–1847. [\[CrossRef\]](#)
13. Shaha, S.K.; Czerwinski, F.; Kasprzak, W.; Friedman, J.; Chen, D.L. Effect of Zr, V and Ti on hot compression behavior of the Al–Si cast alloy for powertrain applications. *J. Alloys Compd.* **2014**, *615*, 1019–1031. [\[CrossRef\]](#)
14. Choi, S.W.; Kim, Y.M.; Lee, K.M.; Cho, H.S.; Hong, S.K.; Kim, Y.C.; Kang, C.S.; Kumai, S. The effects of cooling rate and heat treatment on mechanical and thermal characteristics of Al–Si–Cu–Mg foundry alloys. *J. Alloys Compd.* **2014**, *617*, 654–659. [\[CrossRef\]](#)
15. Sepehrband, P.; Mahmudi, R.; Khomamizadch, F. Effect of Zr addition on the aging behavior of A319 aluminum cast alloy. *Scr. Mater.* **2005**, *52*, 253–257. [\[CrossRef\]](#)
16. Zeren, M. The effect of heat-treatment on aluminum-based piston alloys. *Mater. Des.* **2007**, *28*, 2511–2517. [\[CrossRef\]](#)
17. Teng, D.; Zhang, G.Z.; Zhang, S.; Li, J.W.; Jia, H.F.; He, Q.; Guan, R.G. Microstructure evolution and strengthening mechanism of A356/Al–X–Ce(Ti, C) system by inoculation treatment. *J. Mater. Res. Technol.* **2024**, *28*, 1233–1246. [\[CrossRef\]](#)
18. Li, R.; Du, Z.H.; Yang, H.; He, L.M.; Cui, X.H. Microstructure evolution of 5052 aluminum alloy after electromagnetic-driven stamping following different heat treatment conditions. *J. Mater. Res. Technol.* **2024**, *30*, 485–494. [\[CrossRef\]](#)
19. Jia, Z.H.; Zhou, G.W.; Zhou, H.Y.; Liu, F.; Ding, L.P.; Weng, Y.Y.; Xiang, K.Y.; Zhao, H.D. Effects of Cu content and heat treatment process on microstructures and mechanical properties of Al–Si–Mg–Mn–xCu cast aluminum alloys. *Trans. Nonferrous Met. Soc. China.* **2024**, *34*, 737–754. [\[CrossRef\]](#)
20. Shin, D.; Shyam, A.; Lee, S.; Yamamoto, Y.; Haynes, J.A. Solute segregation at the Al/ θ' -Al₂Cu interface in Al–Cu alloys. *Acta Mater.* **2017**, *141*, 327–340. [\[CrossRef\]](#)
21. Huang, C.L.; Shuai, S.S.; Wang, J.; Shi, L.; Li, S.L.; Nan, R.B.; Li, C.J.; Wang, J.; Ren, Z.M. Magnetic field-induced variation of solid/liquid interfacial energy of solid Al₂Cu and Al–Cu eutectic melt. *J. Alloys Compd.* **2024**, *941*, 168977. [\[CrossRef\]](#)
22. Chen, Y.; Zhang, Z.; Chen, Z.; Tsalanidis, A.; Weyland, M.; Findlay, S.; Allen, L.J.; Li, J.; Medhekar, N.V. The enhanced theta-prime (θ') precipitation in an Al–Cu alloy with trace Au additions. *Acta Mater.* **2017**, *125*, 340–350. [\[CrossRef\]](#)

23. Sandoval, J.H.; Garza, G.H.; Samuel, A.M.; Valtierra, S.; Samuel, F.H. The ambient and high temperature deformation behavior of Al₂SiCuMg alloy with minor Ti, Zr, Ni additions. *Mater. Des.* **2014**, *58*, 89–101. [[CrossRef](#)]
24. Feng, J.; Ye, B.; Zuo, L.; Bao, Q.; Kong, X.; Jiang, H.; Ding, W. Effects of Ni content on low cycle fatigue and mechanical properties of Al-12Si-0.9Cu-0.8Mg-xNi at 350 °C. *Mater. Sci. Eng. A* **2017**, *706*, 27–37. [[CrossRef](#)]
25. Milligan, B.; Ma, D.; Allard, L.; Clarke, A.; Shyam, A. Dislocation- θ' (Al₂Cu) interactions during creep deformation of an Al-Cu alloy. *Scr. Mater.* **2022**, *217*, 114739. [[CrossRef](#)]
26. Li, M.X.; Yang, W.K.; Tian, X.L.; Chen, L.W.; Hou, H.; Zhao, Y.H. Precipitation and refining of Al₂Cu in graphene nanoplatelets reinforced 2024 Al composites. *Mater. Charact.* **2023**, *200*, 112854. [[CrossRef](#)]
27. Ehlers, F.J.; Wenner, H.S.; Andersen, S.J.; Marioara, C.D.; Lefebvre, W.; Boothroyd, C.B.; Holmestad, R. Phase stabilization principle and precipitate host lattice influences for AlMgSiCu alloy precipitates. *J. Mater. Sci.* **2014**, *49*, 6413–6426. [[CrossRef](#)]
28. Veiga, R.; Bellon, B.; Papadimitriou, I.; Manzanares, G.E.; Sabirov, I.; LLorca, J. A multidisciplinary approach to study precipitation kinetics and hardening in an Al-4wt.%Cu alloy. *J. Alloys Comp.* **2018**, *757*, 504–519. [[CrossRef](#)]
29. Sui, Y.; Han, L.; Wang, Q. Effects of thermal exposure on the microstructure and mechanical properties of Al-Si-Cu-Ni-Mg-Gd alloy. *J. Mater. Eng. Perform.* **2019**, *28*, 908–915. [[CrossRef](#)]
30. Farkoosh, A.R.; Pekguleryuz, M. Enhanced mechanical properties of an Al-Si-Cu-Mg alloy at 350 °C: Effects of Mg and the Q-precipitate phase. *Mater. Sci. Eng. A* **2015**, *621*, 277–286. [[CrossRef](#)]
31. Tian, L.H.; Guo, Y.C.; Li, J.P.; Wang, J.L.; Duan, H.B.; Liang, M.X. Elevated re-aging of a piston aluminium alloy and effect on the microstructure and mechanical properties. *Mater. Sci. Eng. A* **2018**, *738*, 375–379. [[CrossRef](#)]
32. Bourgeois, L.; Dwyer, C.; Weyland, M.; Nie, J.F.; Muddle, B.C. The magic thicknesses of θ' precipitates in Sn-microalloyed Al-Cu. *Acta Mater.* **2012**, *60*, 633–644. [[CrossRef](#)]
33. Zhao, Y.H.; Liao, X.Z.; Jin, Z.; Valiev, R.Z.; Zhu, Y.T. Microstructures and mechanical properties of ultrafine grained 7075 Al alloy processed by ECAP and their evolutions during annealing. *Acta Mater.* **2004**, *52*, 4589–4599. [[CrossRef](#)]
34. Ivanisenko, Y.; Lojkowski, W.; Valiev, R.Z.; Fecht, H.J. The mechanism of formation of nanostructure and dissolution of cementite in a pearlitic steel during high pressure torsion. *Acta Mater.* **2005**, *51*, 5555–5570. [[CrossRef](#)]
35. Wang, H.; Qin, G.L.; Li, C.G.; Liang, G.D. Effect of deformation parameters and Al₂Cu evolution on dynamic recrystallization of 2219-O Al alloy during hot compression. *J. Mater. Res. Technol.* **2023**, *26*, 4093–4106. [[CrossRef](#)]
36. Chen, C.L.; Richter, A.; Thomson, R.C. Investigation of mechanical properties of intermetallic phases in multi-component Al-Si alloys using hot-stage nanoindentation. *Intermetallics* **2010**, *18*, 499–508. [[CrossRef](#)]

Disclaimer/Publisher's Note: The statements, opinions and data contained in all publications are solely those of the individual author(s) and contributor(s) and not of MDPI and/or the editor(s). MDPI and/or the editor(s) disclaim responsibility for any injury to people or property resulting from any ideas, methods, instructions or products referred to in the content.